4.2 Related Work

In order to place our data in context, we present some results from work done by groups that have studied different collision systems with similar apparatus. The common thread among these examples is the measurement of soft electrons correlated to momentum transfer to the recoil ion or projectile. As described in the first chapter, the behavior of the three bodies involved in the soft electron production is highly dependent upon the collision system. We present different examples that cover a wide range of ionizing projectiles, divided into groups based primarily upon their projectile velocity regime. These examples include projectile velocities that range from extremely low to very relativistic collisions, and will serve to place our results in the context of existing work. It is important to note this field is relatively young, and all of these results date from within the last few years.

4.2.1 Low velocity collision

We begin with ionization of helium by slow moving ions, such that the projectile velocity is approximately equal to or less than that of the target electron. Note that in this case, due to the low velocity, there is a more substantial longitudinal momentum transfer from the projectile (eq. 4.5). Furthermore, because the projectile takes more time to pass by the target, a large transverse projectile momentum transfer may take place.

These systems were studied extensively with momentum imaging by M. A.

Abdallah during his dissertation research [1.21, 4.1- 4.4]. In addition, groundbreaking work in this field was done by R. Dörner in Frankfurt, Germany [1.20]. Typical results from a low velocity collision measurement are presented in figure 4.1. The spectra shown are views of two dimensions of the electron momentum lying in the collision plane and perpendicular to the collision plane (as defined by the recoil-ion momentum). The two collision systems are singly and doubly charged helium projectiles colliding with a helium target at velocities less than one atomic unit.

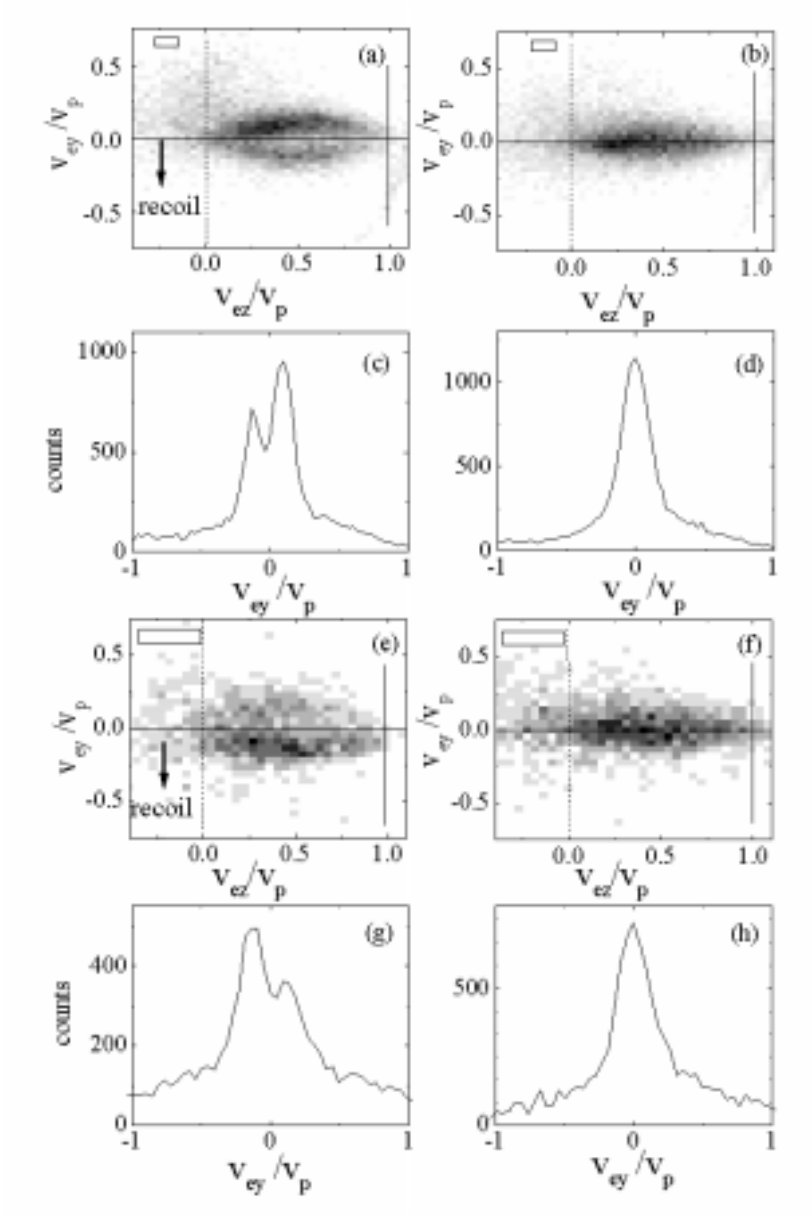

Figure 4.1: (Data from Abdallah [4.4]) (a) Top view and (b) side view of the emitted electrons in the collision v_p = 0.64 a.u. He^+ + He. (c) and (d) are transverse projections of (a), (b) near v_{ez}/v_p = 0.5. (e) and (f) are, respectively, top view and side view of the emitted electrons in the collision v_p = 0.55 a.u. He^{2+} with He, and g) and (h) are the corresponding projections. The approximate resolution functions in the two-dimensional distributions are represented by black rectangles.

There are two significant trends in the low velocity regime that may be seen in this example. The first is that the electrons are pulled forward by the charge of the receding projectile so that their longitudinal momentum is in general positive. In the present example, the electron distributions are spread over velocities between zero and the beam velocity, as if the projectile and target nuclei are sharing the electrons in momentum space. In fact, the nodal structure strongly suggests the formation of a quasi-molecule during the collision.

The other point of significance is that the strongest transverse momentum exchange occurs between the projectile and the recoil ion. In the example presented, the authors measured transverse recoil-ion momenta as large as 15 a.u. Because the transverse electron momentum is barely significant in comparison, we that see in this case the majority of transverse recoil momentum must be balanced by the scattering of the projectile, implying that the strongest transverse momentum exchange is between the projectile and recoil ion, or of "nuclear" type.

4.2.2 Ultra-high velocity collisions/ photoionization

We now take a look at the opposite situation: single ionization by very fast projectiles. Two recent experiments provide excellent examples of the behavior of such systems. The first is a work done using a technique similar to ours by R. Moshammer and J. Ullrich at GSI, Germany [4.5]. They studied single ionization in the collision system 1 GeV/a.m.u. U^{92+} + He, which corresponds to a relativistic ion

velocity of 120 a.u. (0.88c). In this extreme case, the time in which the projectile passes by the target is much shorter than the response time of either the electron or the target nucleus. The result is that there is no significant post-collision effect. The fast pulse of electric field generated by the ion behaves in a manner virtually identical to that of a light-pulse with the electric field vector transverse to the beam axis. This idea is not new; it is generally credited to C. F. Weizacker and E. J. Williams [1.3]. Therefore, nearly no momentum is transferred from the projectile to the target.

This effect is seen in figure 4.2. The horizontal axis of the graph is defined by the projectile beam direction. The vertical axis is chosen to be the direction of the transverse recoil momentum for each event. This is analagous to the collision plane figures shown in preceding low veloctiy example. It is interesting to point out that the location of the projectile momentum on this graph would be 7.5 feet to the right of the figure. Plotted in the figure are the transverse and longitudinal compontents of the recoil momentum, and the electron momentum projected into the same plane. Note that any electron momentum in the plane is balanced by an equal and opposite recoil-ion momentum, which indicates that virtually no momentum is transferred from the projectile. The direction of the electric field pulse (or equivilently, the polariztion vector of the virtual photon) due to the projectile is therefore in the vertical direction.

Another example closely related to the ultra-fast ions is that of photoioniztion. In addition to the measurements of photoionization of D_2 discussed in chapter 3, Doerner *et al.* have also measured the photionization of He [4.6-4.9]. Figure 4.4 is a

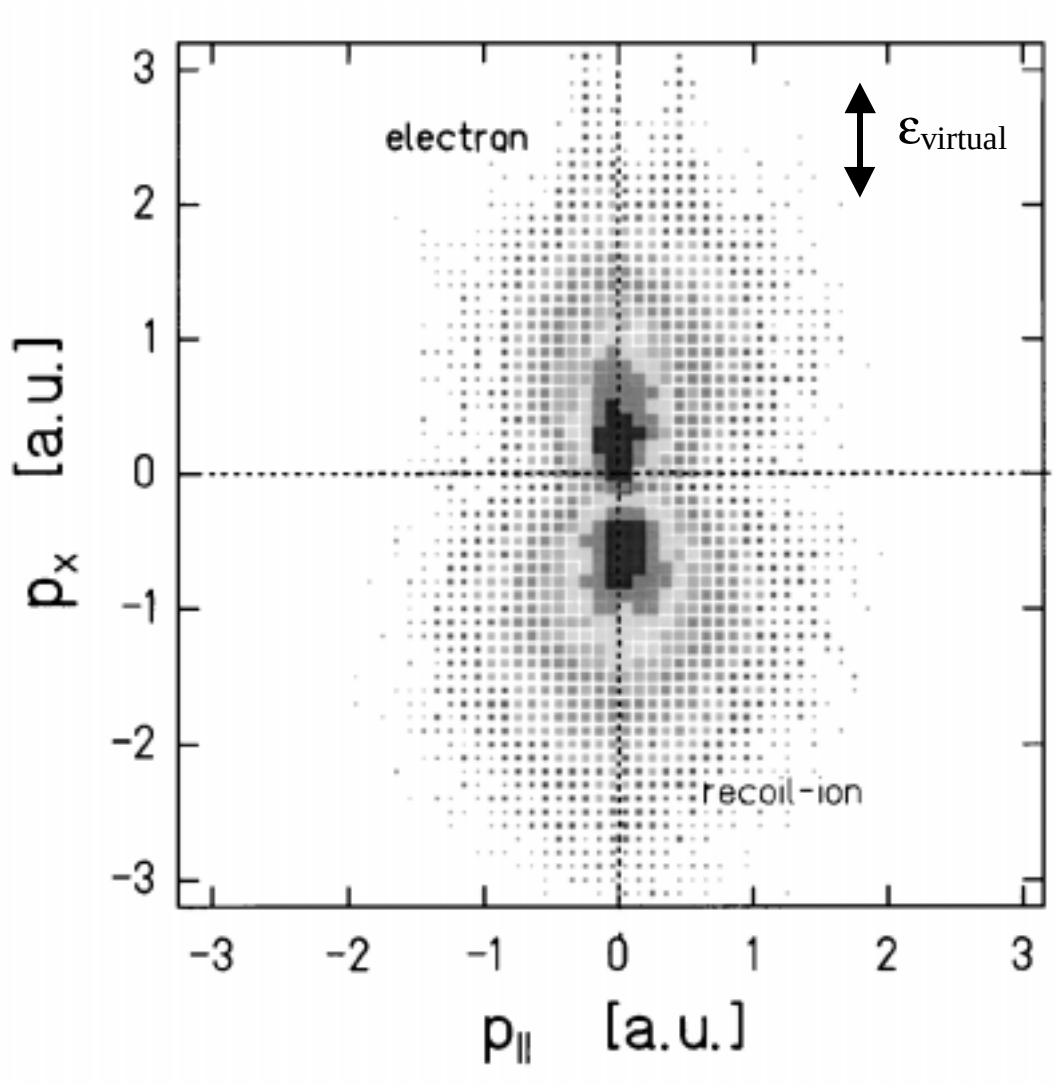

Figure 4.2: (Data by Moshammer [4.5]) Momentum distribution of the electron and the recoiling target ion projected onto the collision plane for 1 GeV/nucleon U^{92+} on He singly ionizing collisions.

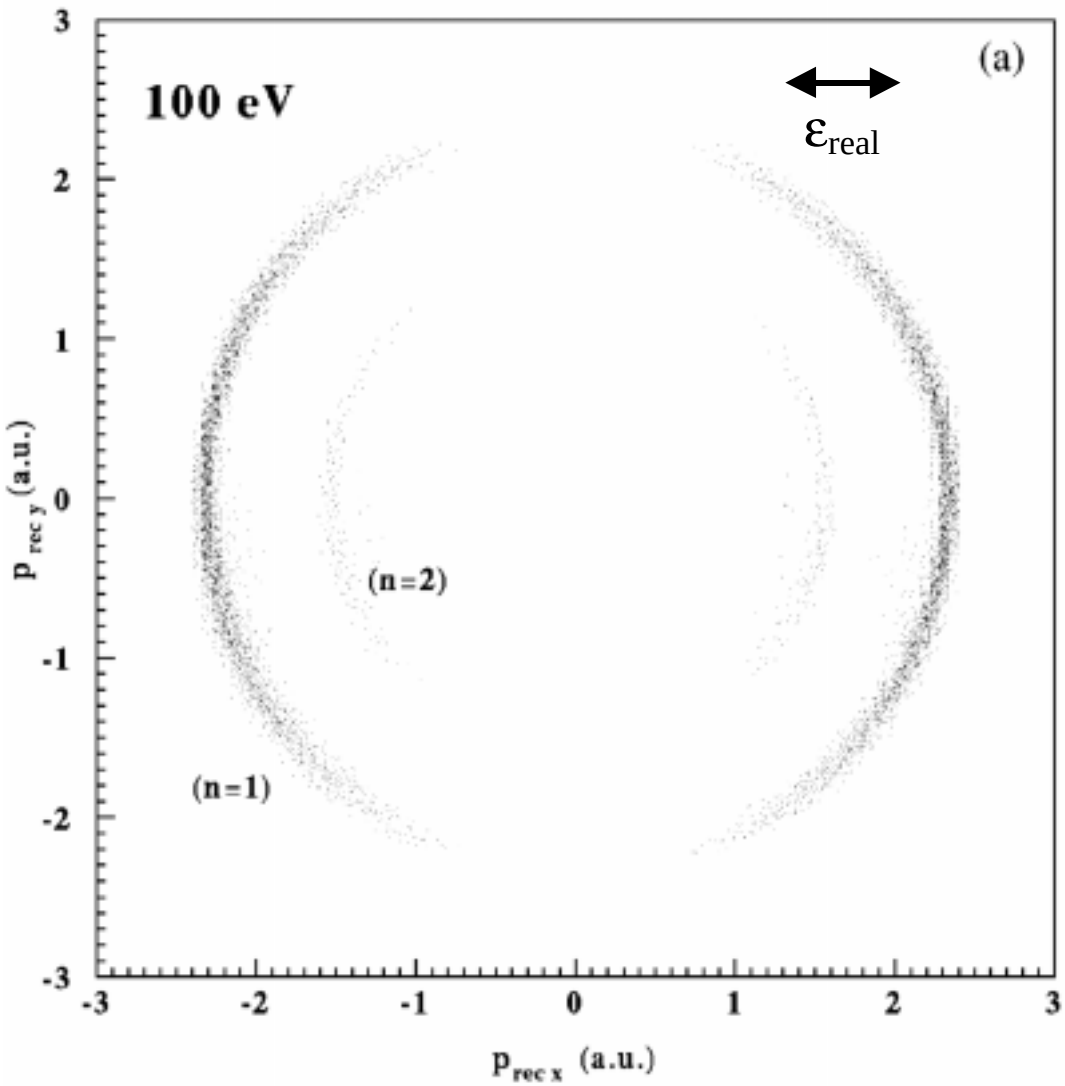

Figure 4.3: (Data by Dorner [4.8]) Transverse momentum distributions for singly-photoionized helium recoil ions. The inner ring corresponds to events where in addition to the ionization, the second electron is promoted to the n=2 state. The continuum electron spectrum would appear as a mirror image due to momentum conservation.

density plot of recoiling He^+ ions. In this case the polarization vector defines the horizontal axis, and the vertical axis is defined by the target jet in the laboratory. The data were integegrated over a small slice (±0.3 a.u.) about zero in the third direction. Because the photon carries very little momentum, the electron spectrum would be identical by inference.

Figures 4.2 and 4.3 are very closely related. Both show that the electrons and recoil ions are ejected in a dipole pattern along the electric field vector in both the relativistic ion-atom collision and the photon-atom collision. In the case of photoionzation, the photon is absorbed, and the *energy* transferred to the target is fixed. This forces the electrons and recoil ions to have quantized momenta, corresponding to the final state of the remaining bound electron. In the case of the ion-atom collision, the energy transferred from the projectile can vary, depending upon the impact parameter in the collision. Therefore, the distributions of electron and recoil momenta are continuous. It is due to this correspondence that we refer to a strong electron-recoil transverse momentum exchange as “photoionization-like”.

4.2.3 High velocity collisions

In a somewhat less extreme case of fast-ion induced ionization, N. Stolterfoht used traditional electron spectroscopy techniques to measure electrons produced in collisions between 95 MeV/a.m.u. bare argon projectiles and lithium atoms [4.10]. In the low velocity and ultra-high velocity examples, we concluded that

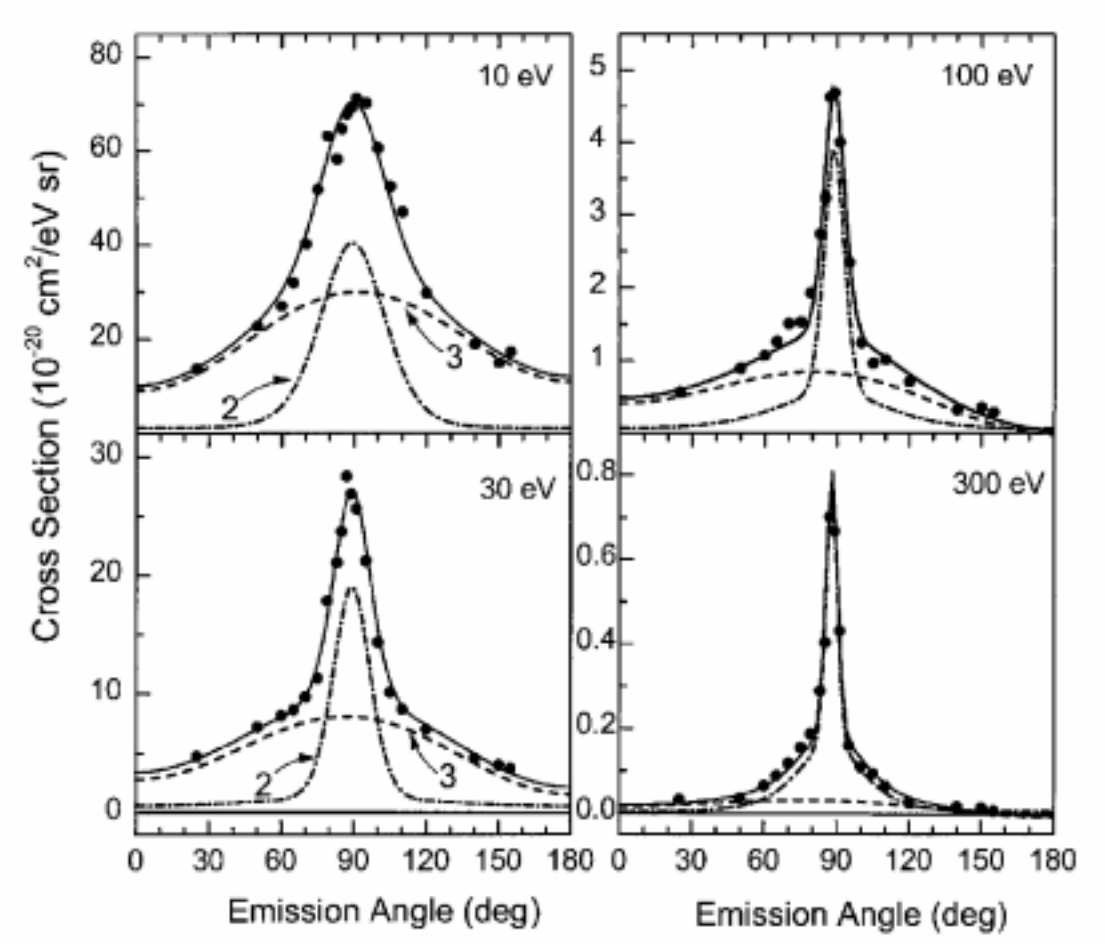

Figure 4.4: (Data by Stolterfoht [4.10]) Angular distributions of electrons emitted at energies of 10, 30, 100, and 300 eV. The dot-dashed curve labeled 2 refers to calculations using a two-body theory. The dashed curve labeled 3 is a fit to the underlying three-body portion using the extended dipole term $A + B\sin^2\theta + C\cos\theta$. The solid curve is the sum of the two dashed curves.

there was clearly only one dominant momentum exchange in each system. For the low velocity case, the dominant exchange was nuclear, and in the ultra-high velocity case, the dominant momentum exchange was "photoionization-like." In this case, however, there is clear evidence of *two* different ionization mechanisms, which correspond to different momentum exchange partners.

Figure 4.4 shows the angular distributions of the electrons in the laboratory frame. In this case, 90° corresponds to electrons ejected perpendicular to the beam axis. The spectra are fitted with two curves designated by the authors as "two-body" and "three-body." These curves were produced by assuming that two distinct mechanisms contribute to the ionization cross section. Details on the determination of these curves may be found in the article.

In describing the two mechanisms, the the term "two-body" refers to a hard collision between the projectile and the electron corresponding to our classification of "binary encounter." Due to the mass difference between the projectile and electron, the elastic collision between the quasi-free electron and projectile forces the ejected electron to lie along a circle in velocity space centered at (and with a radius equal in magnitude to) the projectile velocity. For the relatively low energy electrons in the present example, this corresponded to ejection at 90° to the beam axis.

The second mechanism is, by our terminology, a "photoionization-like" interaction. The authors prefer the term "three-body," in reference to the exchange of a virtual photon between the projectile and the two constituents (electron and recoil ion) of the target. By fitting a sum of the theoretical curves corresponding to the two

mechanisms, they were able to match the data quite well. The relevant case for our soft electron measurements is shown in the 10 eV figure. Even in this case, both mechanisms for soft electron production are apparent.

4.2.4 Trends, intermediate case ⇒ our project.

From these data, there is ample evidence to suggest that in general, the following trends hold true. At low projectile velocities, the electrons are distributed throughout the region between the target and projectile in momentum space, and the transverse momentum is primarily exchanged between the projectile and target nucleus. At extremely high projectile velocities, the projectile interacts with the entire atom in much the same manner as a photon; in both cases the continuum electrons remain local to the target in momentum space and exchange momentum (transverse *and* longitudinal) only with the recoiling target nucleus. At high velocities (yet not so extreme) the electrons can exchange momentum with either the projectile ("two-body"/binary encounter) or the target nucleus ("three-body"/photoionization-like). The question then arises, what of the case of intermediate velocity? One would presume that at some intermediate range, all of these processes would contribute to the production of soft electrons. The major thrust of this experiments described in this chapter was to investigate this point.

One of the few examples at intermediate velocity in the literature is work done by the GSI group, in which they measured ionization of He by 3.6 MeV/a.m.u Se^{28+} [4.11]. This corresponds to a projectile velocity of 12 a.u., which is close to the

regime in which we did our measurements (6.3 to 14 a.u.). However, the high charge on their projectile leads to a ratio of projectile charge to velocity (Z/v) of 2.33, whereas the highest value of this ratio for our experiments was 1.42. This is significant because the first-order interaction strength varies with the ratio Z/v. Shown in figure 4.5 are density plots of the Se^{28+} data by the GSI group. The upper left-hand plot shows the recoil and electron momentum in the collision plane, as defined by the recoil and projectile final momentum vectors. The projectile momentum projected into the same plane is shown in the upper right-hand plot, while the correlation between electron and recoil transverse momentum is shown in the lower plot. As can be seen from the figures, there is a clear momentum balance between the electron and recoil ion in this case. There is a slight scattering of the projectile relative to the recoil ion, but by far the most pronounced effect is the balance of the recoil and electron momentum. In fact the only strong apparent distinction between this data and the ultra-relativistic case is the evidence of the post-collision effect, where the longer collision time allows electron to gain forward momentum and the recoil ion to gain backward momentum from the receding projectile. This effect makes the dipole pattern appear to rotate. The logical inference is that at this projectile charge and velocity, the collisional behavior is primarily photoionization-like. However, as we know from the data in section 4.2.1, at some lower velocity, projectile-recoil momentum exchange must become dominant.

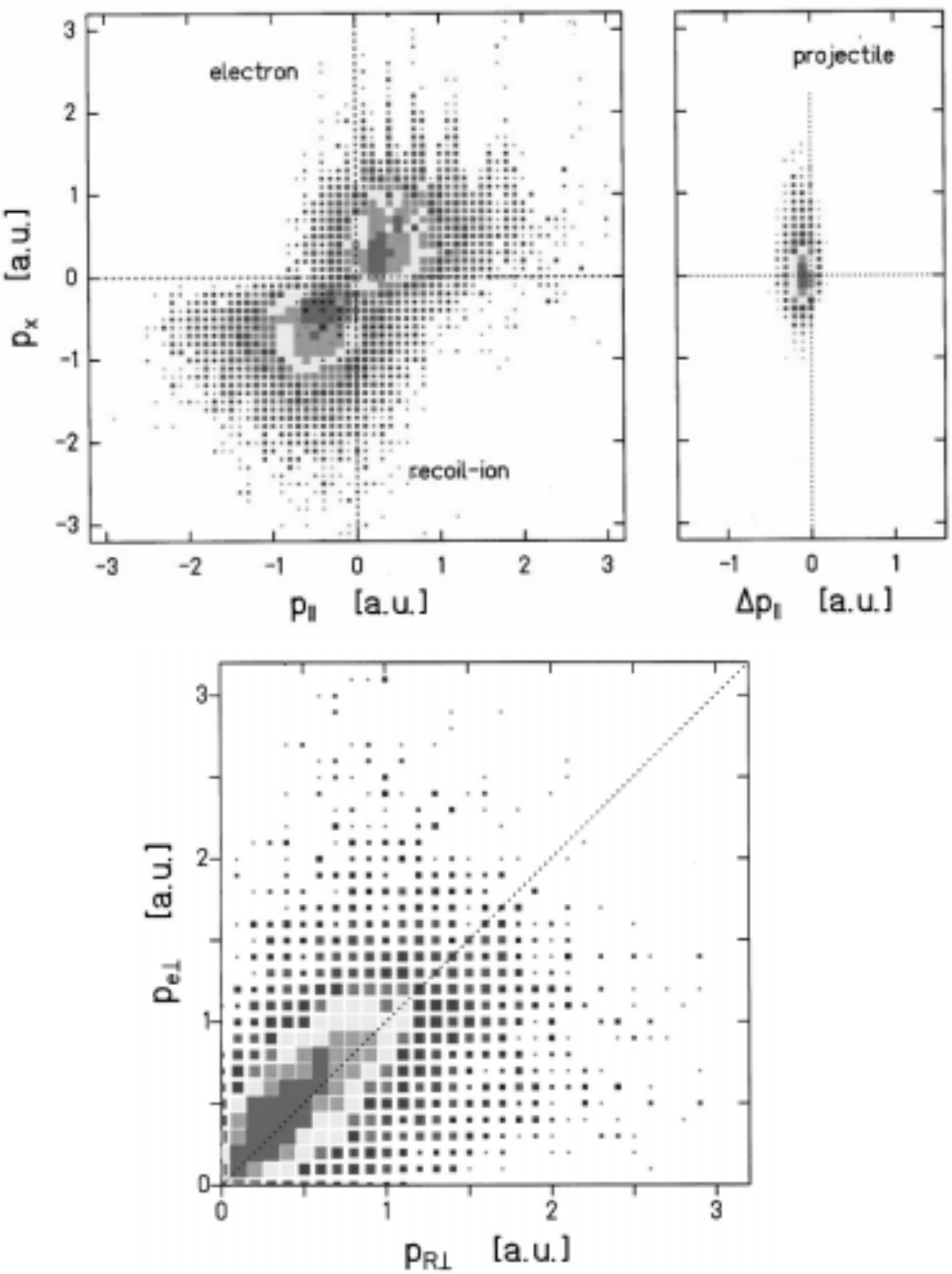

Figure 4.5: (Data by Moshammer [4.11]) Doubly differential cross sections for the collision system 3.6 MeV/a.m.u Se^{28+} + He. Upper left: electron and recoil momentum in the scattering plane. Upper right: projectile momentum in the scattering plane. Bottom: correlation of electron and recoil ion transverse momentum.

4.2.5 Perspective

The measurements we present in this chapter are of three different collision systems that encompass a wide range of projectile charge and velocity. Shown below is a table of the projectiles, velocities and ratio Z/v:

System	Velocity	Charge	Ratio (Z/v)
5 MeV H^+ + He	14.1 a.u.	1	0.07
1 MeV H^+ + He	6.3 a.u.	1	0.15
1 MeV/amu F^{9+} + He	6.3 a.u.	9	1.42

In order to place the above systems in the context of the work of Abdallah *et al.* (Fig. 4.1), we present figure 4.6. It is a density plot of our measurement 1 MeV H^+ electron distribution in the collision plane defined by the transverse recoil ion momentum and the beam axis. The vertical lines on the page represent the projectile and target rest frames. The large circle lies along the classical binary encounter ridge, corresponding to allowed momenta for quasi-free target electrons elasticly scattered by hard two-body collisions with the projectile. The data shown is representative of the region of momentum space that is probed by our measurements.

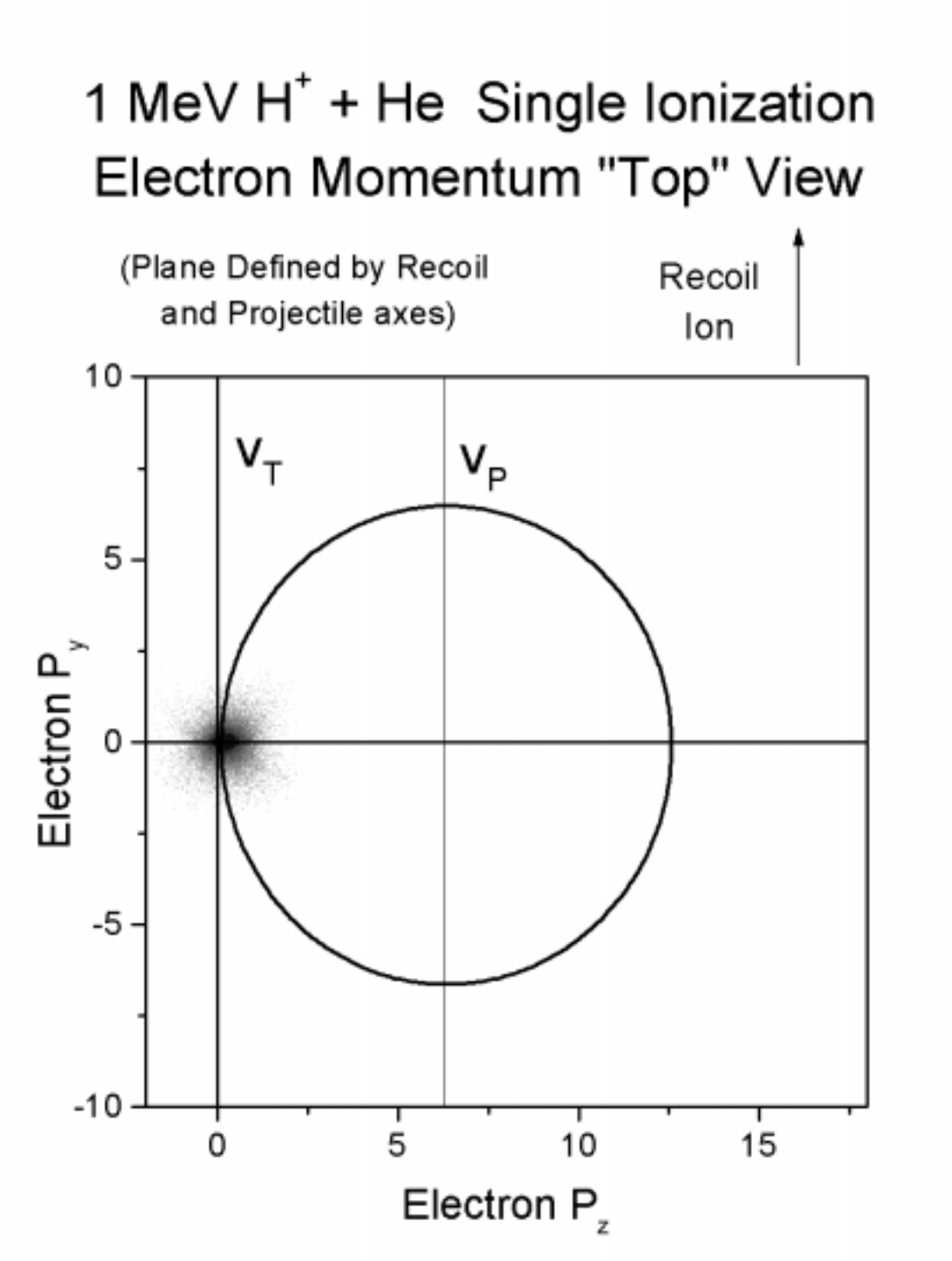

Figure 4.6: Momentum for electrons ejected by 1 MeV protons in the scattering plane defined by the recoil and projectile momentum. The vertical lines represent the projectile and target rest frames. The circle lies along the binary encounter ridge defined by elastic scattering between the projectile and an electron.